


## Generation of cross-cross resonance gates with two fluxonium qubits

Xinpeng Chen(陈鑫鹏) and Zeliang Xiang(项泽亮)
**Citation:**Chin. Phys. B, 2026, 35 (**4**): 040308. DOI: 10.1088/1674-1056/ae13ea
http://cpb.iphy.ac.cn; http://iopscience.iop.org/cpb

**What follows is a list of articles you may be interested in**

---

## Distributed Kuperberg's algorithm

Peng-Yu Yang(杨鹏宇), Xin Zhang(张新), and Song Lin(林崧)
Chin. Phys. B, 2026, 35 (**3**): 030303. DOI: 10.1088/1674-1056/adfb58

## Estimating quantum coherence using limited quantum resources

Bin Zou(邹斌), Kai Wu(吴凯), and Zhihua Chen(陈芝花)
Chin. Phys. B, 2026, 35 (**3**): 030301. DOI: 10.1088/1674-1056/adfb56

## Geometric control of concurrence and quantum gate operations in triangular triple quantum dots

Junqing Li(李俊青), Shuo Dong(董硕), and Jianhua Wei(魏建华)
Chin. Phys. B, 2026, 35 (**2**): 020302. DOI: 10.1088/1674-1056/adec5d

## Impact of surface passivation on the electrical stability of strained germanium devices

Zong-Hu Li(李宗祜), Mao-Lin Wang(王茂鄰), Zhen-Zhen Kong(孔真真), Gui-Lei Wang(王桂磊), Yuan Kang(康原), Yong-Qiang Xu(徐永强), Rui Wu(吴睿), Tian-Yue Hao(郝天岳), Ze-Cheng Wei(魏泽成), Bao-Chuan Wang(王保传), Hai-Ou Li(李海欧), Gang Cao(曹刚), and Guo-Ping Guo(郭国平)
Chin. Phys. B, 2025, 34 (**9**): 090305. DOI: 10.1088/1674-1056/add4de

## Domain adaptation method inspired by quantum convolutional neural network

Chunhui Wu(武春辉), Junhao Pei(裴骏豪), Yihua Wu(吴逸华), Anqi Zhang(张安琪), and Shengmei Zhao(赵生妹)
Chin. Phys. B, 2025, 34 (**7**): 070302. DOI: 10.1088/1674-1056/adc7ed

---

# Generation of cross-cross resonance gates with two fluxonium qubits

Xinpeng Chen(陈鑫鹏)† and Zeliang Xiang(项泽亮)

*School of Physics, Sun Yat-sen University, Guangzhou* 510275, *China*

(Received 11 April 2025; revised manuscript received 26 August 2025; accepted manuscript online 16 October 2025)

The cross-cross resonance (CCR) gate is an extension of the cross-resonance (CR) gate that has been theoretically implemented with transmon qubits. However, the weak anharmonicity of transmon qubits leads to decoherence and leakage errors, which reduce the fidelity of the gate operation. In this work, we propose employing fluxonium qubits to implement the CCR gate. With similar drive amplitudes, our scheme can achieve the required stronger $ZX$ and $XZ$ interactions compared to a transmon qubit system, resulting in shorter gate times. By combining the CCR gate with specific single-qubit gates, a $\sqrt{\text{iSWAP}}$ gate is realized, thereby enabling the construction of the iSWAP and SWAP gates. Moreover, through parameter optimization, these gates built on fluxonium qubits exhibit a significant reduction in operation time while simultaneously achieving higher fidelity. Our results provide valuable insights into achieving fast, low-error-rate swapping operations in superconducting circuits.

**Keywords:** quantum computing, superconducting qubit, quantum gate

**PACS:** 03.67.Lx, 03.65.Aa, 85.25.Am

**DOI:** 10.1088/1674-1056/ae13ea **CSTR:** 32038.14.CPB.ae13ea

## 1. Introduction

In recent years, superconducting circuits have become one of the main platforms for quantum information processing.[1–4] Superconducting qubits in these circuits can be classified into charge qubits,[5,6] flux qubits,[7,8] and phase qubits[9,10] based on the ratio of Josephson energy $E_{\rm J}$ to charging energy $E_{\rm C}$.[11] To date, the most widely adopted superconducting qubit is the transmon, which was developed from the charge qubit.[12,13] Although the condition $E_{\rm J}/E_{\rm C} \gg 1$ endows the transmon qubit with insensitivity to charge noise, it also results in weak anharmonicity, which leads to state leakage and reduces the fidelity of gate operations. Recently, the fluxonium qubit has emerged as a competitive candidate for quantum computing in superconducting circuits.[14–18] A standard fluxonium qubit consists of a large Josephson junction inductively shunted by an array composed of $N \approx 100$ junctions. Its circuit topology is inspired by the flux qubit design but features a substantially larger inductor, resulting in a strongly nonlinear energy spectrum and a lower dephasing rate.[15] This inherent property can be leveraged to mitigate the impact of flux noise even when the operation is not performed at the sweet spot.[3,14] State-of-the-art experiments with fluxonium qubits have demonstrated single-qubit gate fidelities exceeding 99.997%[19] and single-shot readout fidelities of 97.8%.[20]

To implement a wide range of quantum logic operations, it is essential to have a set of single- and two-qubit gates.[21] Within superconducting quantum circuits, high-fidelity single-qubit gates can be realized through pulse-driven manipulation of individual qubits, while two-qubit gates are generally created by inducing interactions between qubits and performing appropriate controls. Among various methods, the cross-resonance (CR) gate is particularly promising due to its flexibility and simplicity. It only requires microwave pulses to drive qubits, avoiding the introduction of flux noise into the system.[22,23] The CR gate finds wide applications in many domains of quantum computing, such as quantum error correction,[24,25] quantum simulation,[26] and quantum algorithms.[27] The key idea of the CR gate is to induce the $ZX$ interaction by driving the control qubit at a frequency resonant with the target qubit. This $ZX$ interaction can serve as a fundamental component for generating other two-qubit gates, such as the controlled-NOT (CNOT) gate.[28–30] Currently, the CNOT gate with a fidelity exceeding 99% has been realized using the CR gate.[31–33] The method of the cross-cross resonance (CCR) gate is similar to that of the CR gate, except that the target qubit in the CCR gate is driven by an additional pulse resonant with the control qubit. This design gives rise to both $ZX$ and $XZ$ interactions, enabling the implementation of iSWAP and SWAP gates when combined with specific quantum gates, such as rotation gates. Theoretically, CCR gates have been employed to realize an iSWAP gate with an operation time of 647.1 ns and a SWAP gate with an operation time of 935.1 ns using transmon qubits.[34] Meanwhile, lower error rates are achieved compared with the CR gate scheme under similar conditions. However, this CCR gate scheme is based on transmon qubits, and their inherent drawbacks are inevitably introduced into the gate operation.[17,35] How to mitigate these drawbacks and improve the performance of CCR gates remains an open question.

In this paper, we study the CCR gate using two fluxonium qubits with distinct frequencies. The qubits are capac-

†Corresponding author. E-mail: 1594729446@qq.com

© 2026 Chinese Physical Society and IOP Publishing Ltd. All rights, including for text and data mining, AI training, and similar technologies, are reserved.

itively coupled and individually driven by microwave pulses. By performing the Schrieffer–Wolff (SW) transformations and representing the system in the rotating frame, we derive the effective Hamiltonian, in which the $ZX$ and $XZ$ interactions are stronger than those in the transmon case under similar conditions. This implies that the time required to implement the gate operation is shorter. Meanwhile, the strong anharmonicity of fluxonium qubits reduces both decoherence and noise crosstalk arising from state leakage, enhancing the fidelity of quantum gates. Furthermore, we utilize the CCR gate with optimized parameters to generate iSWAP and SWAP gates. The results of interleaved randomized benchmarking experiments show that, with state-of-the-art experimental parameters, an iSWAP gate with an operation time of 439 ns and a fidelity of 99.5%, along with a SWAP gate with an operation time of 656 ns and a fidelity of 98.3%, can be realized.

The structure of the paper is as follows. In Section 2, we introduce the model of the fluxonium CCR gate and discuss its properties. Then, based on this CCR gate, Section 3 presents the implementation and optimization of the iSWAP and SWAP gates. In Section 4, we analyze the error budget of the $\mathrm{CCR}_{\pi/4}$. Finally, we summarize the main results in Section 5.

## 2. Model

### 2.1. The effective Hamiltonian

As depicted in Fig. 1, we consider a circuit consisting of two fluxonium qubits, which are capacitively coupled and driven by two microwave pulses. This system can be described by the Hamiltonian

$$\hat{H} = \hat{H}_A + \hat{H}_B + \hat{H}_{\mathrm{drive}} + \hat{H}_{\mathrm{int}}, \tag{1}$$

where

$$\hat{H}_{\xi(\xi\in\{A,B\})} = 4E_{\mathrm{C}(\xi)}\hat{n}_\xi^2 - E_{\mathrm{J}(\xi)}\cos(\hat{\varphi}_\xi + \varphi_{e(\xi)}) + \frac{1}{2}E_{\mathrm{L}(\xi)}\hat{\varphi}_\xi^2, \tag{2}$$

$$\hat{H}_{\mathrm{drive}} = E_1\cos(\omega_{d1}t+\phi_1)\hat{n}_A + E_2\cos(\omega_{d2}t+\phi_2)\hat{n}_B, \tag{3}$$

$$\hat{H}_{\mathrm{int}} = J_{\mathrm{C}}\hat{n}_A\hat{n}_B. \tag{4}$$

Here, $\hat{H}_{\xi(\xi\in\{A,B\})}$ denotes the free Hamiltonian of qubit $\xi$. We select the two lowest eigenstates of each fluxonium qubit as the computational basis, with their transition frequencies being $\omega_A$ and $\omega_B$, respectively.[22,23] Without loss of generality, we assume $\omega_A < \omega_B$, so that $\hat{H}_A$ and $\hat{H}_B$ are reduced to

$$\hat{H}_{\xi(\xi\in\{A,B\})} = -\frac{\hbar\omega_\xi}{2}\hat{\sigma}_z^\xi. \tag{5}$$

$\hat{H}_{\mathrm{drive}}$ and $\hat{H}_{\mathrm{int}}$ correspond to the drive Hamiltonian and the interaction Hamiltonian, respectively. $E_{1(2)}\cos(\omega_{d1(2)}t+\phi_{1(2)})$ denotes the microwave pulse applied to qubit $A$ ($B$). $\hat{n}_A$ and $\hat{n}_B$ are the charge operators of the qubits, and $J_{\mathrm{C}}$ denotes the capacitive coupling strength between the two fluxonium qubits. In this work, we set the phase of the drives to $\phi_{1(2)} = 0$.

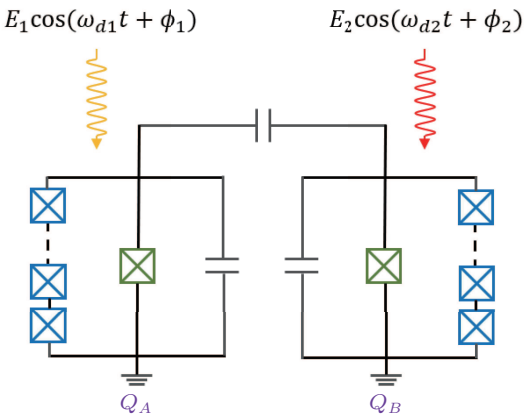



**Fig. 1.** Schematic diagram of the CCR gate based on fluxonium qubits. $Q_A$ and $Q_B$ are two fluxonium qubits capacitively coupled. The orange and red wavy lines represent the microwave drives applied to $Q_A$ and $Q_B$, respectively. The frequencies of the two microwave pulses satisfy the condition for cross-cross resonance.

Now, the system Hamiltonian can be written as

$$\hat{H} = -\frac{\hbar\omega_A}{2}\hat{\sigma}_z^A - \frac{\hbar\omega_B}{2}\hat{\sigma}_z^B + J_{\mathrm{C}}\hat{n}_A\hat{n}_B + E_1\cos(\omega_{d1}t)\hat{n}_A + E_2\cos(\omega_{d2}t)\hat{n}_B. \tag{6}$$

Through the SW transformations and representations in the rotating frame, which are detailed in Appendix A, we obtain the effective Hamiltonian of the system as

$$\begin{aligned}\hat{H}_{\mathrm{eff}} = {} & \frac{E_1}{2}\left(1-\frac{r_2^2}{4}\right)(n^A_{00,01}+n^A_{10,11})\frac{IX}{2} \\ & + \frac{E_2}{2}\left(1-\frac{r_1^2}{4}\right)(n^B_{00,10}+n^B_{01,11})\frac{XI}{2} \\ & + \frac{E_1}{2}\left[\left(1-\frac{r_1^2}{2}-\frac{r_2^2}{4}\right)(n^A_{00,01}-n^A_{10,11}) + \frac{r_2^2}{2}(n^B_{00,10}-n^B_{01,11})\right]\frac{ZX}{2} \\ & + \frac{E_2}{2}\left[\left(1-\frac{r_2^2}{2}-\frac{r_1^2}{4}\right)(n^B_{00,10}-n^B_{01,11}) + \frac{r_1^2}{2}(n^A_{00,01}-n^A_{10,11})\right]\frac{XZ}{2},\end{aligned} \tag{7}$$

where $r_i = E_i/[\hbar(\tilde{\omega}_i - \omega_{di})]$ for $i\in\{1,2\}$, with $\tilde{\omega}_i$ and $\omega_{di}$ being the frequencies of qubit $i$ and the corresponding drive pulse, respectively. $X$, $Y$, and $Z$ denote the Pauli operators $\hat{\sigma}_x$, $\hat{\sigma}_y$, and $\hat{\sigma}_z$. The term $MN$ represents the tensor product of operators $M$ and $N$ ($M,N\in\{I,X,Y,Z\}$) acting on qubits $A$ and $B$, respectively. $n^{A(B)}_{ab,cd}$ denotes the matrix element of the charge operator of qubit $A$ ($B$) between two dressed states $|ab\rangle$ and $|cd\rangle$.

According to Eq. (7), if $E_2 = 0$, the Hamiltonian reduces to

$$\hat{H}_{\mathrm{eff}} = \frac{E_1}{2}\left(1-\frac{r_1^2}{2}\right)(n^A_{00,01}-n^A_{10,11})\frac{ZX}{2}$$

$$+\frac{E_1}{2}(n^A_{00,01}+n^A_{10,11})\frac{IX}{2}. \tag{8}$$

It is evident that the system reduces to a CR gate.

### 2.2. Properties of the fluxonium CCR gate

In the study of the CCR gate, we focus on the $ZX$ and $XZ$ interactions, while demonstrating that the IX and XI terms in the Hamiltonian (7) can be suppressed via active cancellation pulses.[28] Therefore, the Hamiltonian (7) can be rewritten as

$$\begin{aligned}\hat{H}_{\rm eff} =& \frac{E_1}{2}\left[\left(1-\frac{r_1^2}{2}-\frac{r_2^2}{4}\right)(n^A_{00,01}-n^A_{10,11})\right.\\ &\left.+\frac{r_2^2}{2}(n^B_{00,10}-n^B_{01,11})\right]\frac{ZX}{2}\\ &+\frac{E_2}{2}\left[\left(1-\frac{r_2^2}{2}-\frac{r_1^2}{4}\right)(n^B_{00,10}-n^B_{01,11})\right.\\ &\left.+\frac{r_1^2}{2}(n^A_{00,01}-n^A_{10,11})\right]\frac{XZ}{2}.\end{aligned} \tag{9}$$

Then, we facilitate the comparison of gate performance by using KAK decomposition. Generally, a two-qubit gate can be decomposed into the following form:

$$U = q_1 \exp\left(-\mathrm{i}\sum_{i=1}^{3} c_i \frac{Q_i}{2}\right) q_2, \tag{10}$$

where $q_1$, $q_2$, and $Q_i$ are $4\times4$ matrices, and $c_i$ ($i\in\{1,2,3\}$) is the Cartan coefficient.[34] $Q_i$ denotes the tensor product of two Pauli operators. Note that $Q_1$, $Q_2$, and $Q_3$ are mutually commutative.

The evolution of the CCR gate is given by $\exp(-\mathrm{i}\hat{H}_{\rm eff}t)$, from which we can obtain the Cartan coefficients of the fluxonium CCR gate on the basis $\{Q_1,Q_2,Q_3\}=\{ZX,XZ,YY\}$ as

$$\boldsymbol{c}(t) = (c_1(t), c_2(t), c_3(t)), \tag{11}$$

where

$$\begin{aligned}c_1(t) =& \frac{E_1}{2}\left[\left(1-\frac{r_1^2}{2}-\frac{r_2^2}{4}\right)(n^A_{00,01}-n^A_{10,11})\right.\\ &\left.+\frac{r_2^2}{2}(n^B_{00,10}-n^B_{01,11})\right]t,\end{aligned} \tag{12}$$

$$\begin{aligned}c_2(t) =& \frac{E_2}{2}\left[\left(1-\frac{r_2^2}{2}-\frac{r_1^2}{4}\right)(n^B_{00,10}-n^B_{01,11})\right.\\ &\left.+\frac{r_1^2}{2}(n^A_{00,01}-n^A_{10,11})\right]t,\end{aligned} \tag{13}$$

$$c_3(t) = 0. \tag{14}$$

For comparison, the Hamiltonian of the transmon CCR gate is[34]

$$\hat{H}_{\rm tr} = \frac{g'E'_1}{\sqrt{\Delta'^2+E'^2_1+\frac{3}{2}E'^2_2}}\frac{ZX}{2} - \frac{g'E'^2_2}{\sqrt{\Delta'^2+\frac{3}{2}E'^2_1+E'^2_2}}\frac{XZ}{2}, \tag{15}$$

and the corresponding Cartan coefficients are

$$\boldsymbol{c}_{\rm tr}(t) = \left(\frac{g'E'_1}{\sqrt{\Delta'^2+E'^2_1+\frac{3}{2}E'^2_2}}t,\ -\frac{g'E'_2}{\sqrt{\Delta'^2+\frac{3}{2}E'^2_1+E'^2_2}}t,\ 0\right). \tag{16}$$

We then control the evolution time of the CCR gate to obtain

$$\mathrm{CCR}_{\pi/4} = \exp\left[-\mathrm{i}\frac{\pi(ZX-XZ)}{8}\right]. \tag{17}$$

The Cartan coefficients of this gate take the following form:

$$\left(\frac{\pi}{4},\ -\frac{\pi}{4},\ 0\right). \tag{18}$$

If we perform the KAK decomposition of $\mathrm{CCR}_{\pi/4}$ on the basis $\{XX,YY,ZZ\}$, the two-qubit operator can be obtained as

$$\exp\left[\mathrm{i}\frac{\pi(XX+YY)}{8}\right], \tag{19}$$

which is equivalent to a $\sqrt{\mathrm{iSWAP}}$ gate. The details of the decomposition are shown in Fig. 2, from which we can transform the $\mathrm{CCR}_{\pi/4}$ into the $\sqrt{\mathrm{iSWAP}}$ via unitary operations. With such a gate, we can further implement the iSWAP and SWAP gates.

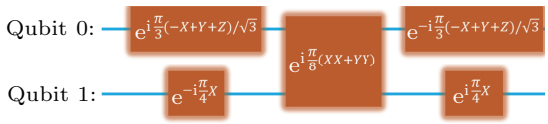



**Fig. 2.** The circuit for the KAK decomposition of $\mathrm{CCR}_{\pi/4}$. The middle segment represents a $\sqrt{\mathrm{iSWAP}}$ gate.

To compare the two schemes under similar conditions, we make the following assumptions:

$$E_1 = \frac{s_2}{s_2-s_1}E,\quad E_2 = -\frac{s_1}{s_2-s_1}E,\quad E'_1 = E'_2 = \frac{E}{2}, \tag{20}$$

where

$$\begin{aligned}s_1 &= \left(1-\frac{r_1^2}{2}-\frac{r_2^2}{4}\right)(n^A_{00,01}-n^A_{10,11})+\frac{r_2^2}{2}(n^B_{00,10}-n^B_{01,11}),\\ s_2 &= \left(1-\frac{r_2^2}{2}-\frac{r_1^2}{4}\right)(n^B_{00,10}-n^B_{01,11})+\frac{r_1^2}{2}(n^A_{00,01}-n^A_{10,11}).\end{aligned} \tag{21}$$

Hence, the drive amplitudes satisfy the equation

$$E_1+E_2 = E'_1+E'_2 = E. \tag{22}$$

The evolution times for the two types of CCR gates can be deduced based on the preceding analysis as

$$t^{\rm fl} = \frac{(s_2-s_1)\pi}{2s_1s_2E}, \tag{23}$$

$$t^{\mathrm{tr}} = \frac{\pi\sqrt{\Delta'^2 + \frac{5}{8}E^2}}{2g'E}, \tag{24}$$

where the superscript 'fl' represents the fluxonium qubit and 'tr' represents the transmon qubit. We find that $t^{\mathrm{fl}} < t^{\mathrm{tr}}$ under the condition $g'/E \ll 1$, confirming that the fluxonium qubit offers a shorter gate duration compared to the transmon qubit for implementing the CCR gate.

## 3. Implementations of the iSWAP and SWAP gates

### 3.1. Optimization of the CCR gate

In our scheme, the implementation of high-performance iSWAP and SWAP gates relies on realizing a high-fidelity and fast CCR gate, whose fidelity is influenced by the gate duration and the frequency detunings between drives and qubits. Due to this complex relationship, comprehensive numerical simulations are performed to determine the optimal configuration that allows the CCR gate to achieve its best performance. We set multiple gate durations and scan across the parameters $M_1 = \omega_{d1} - \tilde{\omega}_2$ and $M_2 = \omega_{d2} - \tilde{\omega}_1$ for each gate duration to identify the maximum fidelity achievable by the CCR gate. The results are shown in Fig. 3, where we observe that the maximum fidelity increases with gate time initially and then remains nearly unchanged, indicating that extending the gate time further does not significantly improve the gate fidelity. Moreover, increasing the gate time may lead to decoherence; therefore, we select $t = 112$ ns as the optimal parameter for the fluxonium CCR gate. The parameters of the two fluxonium qubits are presented in Table 1, and the coupling strength between the two qubits is $J/h = 0.32$ GHz.

**Table 1.** Parameters of qubits.

| | $\omega_{01}/(2\pi)$ (GHz) | $\omega_{12}/\omega_{01}$ | $\alpha/(2\pi)$ (GHz) | $T_1$ (μs) | $T_2$ (μs) |
|---|---|---|---|---|---|
| $A$ | 0.78 | 3.4 | 1.872 | 110 | 160 |
| $B$ | 0.83 | 2.5 | 1.245 | 108 | 140 |

Next, it is necessary to identify the parameter ranges for $M_1$ and $M_2$. In the simulation, the detuning between the two qubits is $\Delta/(2\pi) = (\tilde{\omega}_1 - \tilde{\omega}_2)/(2\pi) \approx -59.32$ MHz, while the amplitudes of the two microwave pulses are

$$\frac{E_1}{\hbar} = \sqrt{\frac{2M_2(M_1-\Delta)}{1+n^A_{00,10}+n^A_{01,11}}},$$
$$\frac{E_2}{\hbar} = \sqrt{\frac{2M_1(M_2+\Delta)}{1+n^B_{00,01}+n^B_{10,11}}}, \tag{25}$$

and satisfy the condition $E_1, E_2 < \hbar|\Delta|$. Given that both $E_1$ and $E_2$ are real numbers, we set $M_1/(2\pi) \in [-45,\ 0]$ MHz and $M_2/(2\pi) \in [0,\ 45]$ MHz, respectively. The coherent fidelity of a unitary evolution $U$ on an $n$-dimensional complex Hilbert space is defined as

$$F = \frac{1}{n(n+1)}\left[\mathrm{Tr}(U^\dagger U) + |\mathrm{Tr}(U_0^\dagger U)|^2\right], \tag{26}$$

where $U_0$ denotes the desired quantum gate. For the CCR gate, which acts on a two-qubit system with Hilbert space dimension $n = 4$, the coherent fidelity is given by

$$F = \frac{\mathrm{Tr}\left(U^\dagger_{\mathrm{CCR}}U_{\mathrm{CCR}}\right) + \left|\mathrm{Tr}\left(U^\dagger_{\mathrm{target}}U_{\mathrm{CCR}}\right)\right|^2}{20}. \tag{27}$$

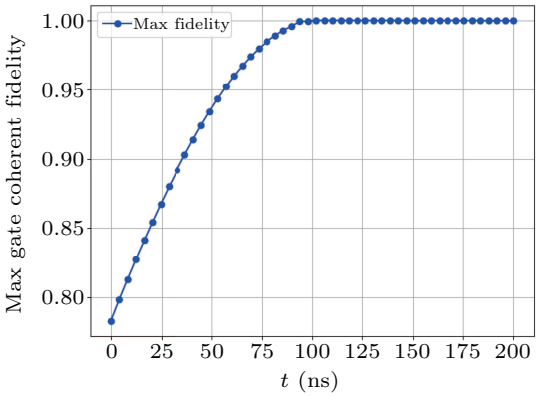



**Fig. 3.** The maximum fidelity at different CCR gate durations. For each gate duration, the fidelities for various configurations of $M_1$ and $M_2$ are calculated, and the maximum value is selected as the data point shown in this figure.

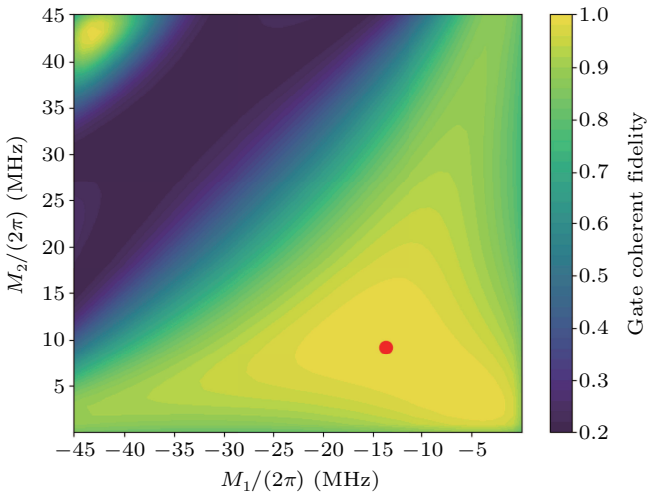



**Fig. 4.** The coherent fidelity of the CCR gate as a function of $M_1$ and $M_2$. The gate time is 112 ns, and the maximum fidelity is achieved at $(-13.78\ \mathrm{MHz}, 9.18\ \mathrm{MHz})$, which is marked with a red dot in the figure.

The result indicates that the maximum fidelity of the CCR gate exceeds 99% at $t = 112$ ns. At this duration, the fidelities of the CCR gate for various configurations $(M_1, M_2)$ are depicted in Fig. 4. From the figure, the CCR gate exhibits higher fidelity when the absolute values of $M_1$ and $M_2$ are both small but nonzero. When $M_1/(2\pi) = -13.78$ MHz and $M_2/(2\pi) = 9.18$ MHz, the fidelity reaches its maximum. The drive frequencies can be determined using the following expressions:

$$\omega_{d1} = M_1 + \tilde{\omega}_2 = 2\pi \times 0.82\ \mathrm{GHz},$$
$$\omega_{d2} = M_2 + \tilde{\omega}_1 = 2\pi \times 4.99\ \mathrm{GHz}. \tag{28}$$

In addition, the drive amplitudes are $E_1/h = 24.2$ MHz and $E_2/h = 30.7$ MHz, where $h$ denotes the Planck constant.

### 3.2. The iSWAP and SWAP gates

The iSWAP and SWAP gates can be decomposed into multiple $\sqrt{\text{iSWAP}}$ gates along with several single-qubit rotation gates, as shown below:[34]

$$U_{\text{iSWAP}} = \left(U_{\sqrt{\text{iSWAP}}} \cdot U_{X+Y} \otimes U_{X+Y}\right)^2,$$
$$U_{\text{SWAP}} = \left(U_{\sqrt{\text{iSWAP}}} \cdot U_{X+Y+Z} \otimes U_{X+Y+Z}\right)^3, \quad (29)$$

where $U_{X+Y} = \mathrm{e}^{\mathrm{i}\frac{\pi}{2}(\sigma_x+\sigma_y)/\sqrt{2}}$ and $U_{X+Y+Z} = \mathrm{e}^{\mathrm{i}\frac{\pi}{3}(\sigma_x+\sigma_y+\sigma_z)/\sqrt{3}}$. The $\sqrt{\text{iSWAP}}$ gate can be obtained from $\text{CCR}_{\pi/4}$ according to Fig. 2

$$U_{\sqrt{\text{iSWAP}}} = (A_1 \otimes B_1) \cdot \text{CCR}_{\pi/4} \cdot (A_2 \otimes B_2), \quad (30)$$

where

$$A_1 = \exp\left(\mathrm{i}\frac{\pi}{3\sqrt{3}}(-X+Y+Z)\right),$$
$$A_2 = \exp\left(-\mathrm{i}\frac{\pi}{3\sqrt{3}}(-X+Y+Z)\right),$$
$$B_1 = \exp\left(-\mathrm{i}\frac{\pi}{4}X\right), \quad B_2 = \exp\left(\mathrm{i}\frac{\pi}{4}X\right). \quad (31)$$

To investigate the properties of the CCR gate, we use Gaussian flat-top pulses to simulate the evolution process

$$f(t) = \frac{f_1(t) - f_1(-1)}{1 - f_1(-1)}, \quad (32)$$

where

$$f_1(t) = \begin{cases} \exp\left[-\frac{1}{2}\left(\frac{t-t_\text{r}}{\sigma}\right)^2\right], & t \in [0,\ t_\text{r}), \\ 1, & t \in [t_\text{r},\ t_\text{d}-t_\text{f}), \\ \exp\left\{-\frac{1}{2}\left[\frac{t-(t_\text{d}-t_\text{f})}{\sigma}\right]^2\right\}, & t \in [t_\text{d}-t_\text{f},\ t_\text{d}]. \end{cases} \quad (33)$$

Here, $t_\text{r}$ and $t_\text{f}$ denote the rise time and fall time of the gate, respectively, $\sigma$ is the standard deviation, and $t_\text{d}$ denotes the total gate duration. We use Qiskit to simulate the pulse for generating $\text{CCR}_{\pi/4}$,[36] and Fig. 5 illustrates the gate process. In our simulation, $t_\text{r} = t_\text{f} = 2\sigma = 18$ ns and $t_\text{d} = 112$ ns.

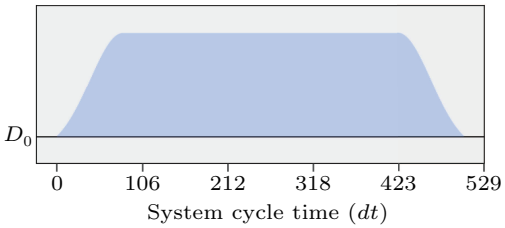



**Fig. 5.** Pulse diagram for the $\text{CCR}_{\pi/4}$ gate. The total duration is 112 ns (504 $dt$), the standard deviation is 9 ns (40.5 $dt$), and the durations of the rise and fall edges are both 18 ns (81 $dt$), with $dt = 0.222$ ns denoting the fundamental cycle time for pulse generation.

To measure the fidelities of the iSWAP and SWAP gates generated with the fluxonium CCR gate, we conduct interleaved randomized benchmarking experiments, and the results are shown in Fig. 6. We find that the fidelity of the iSWAP gate reaches 99.5% with a gate time of 439 ns, while the fidelity of the SWAP gate reaches 98.3% with a gate time of 656 ns. These results are listed in Table 2.

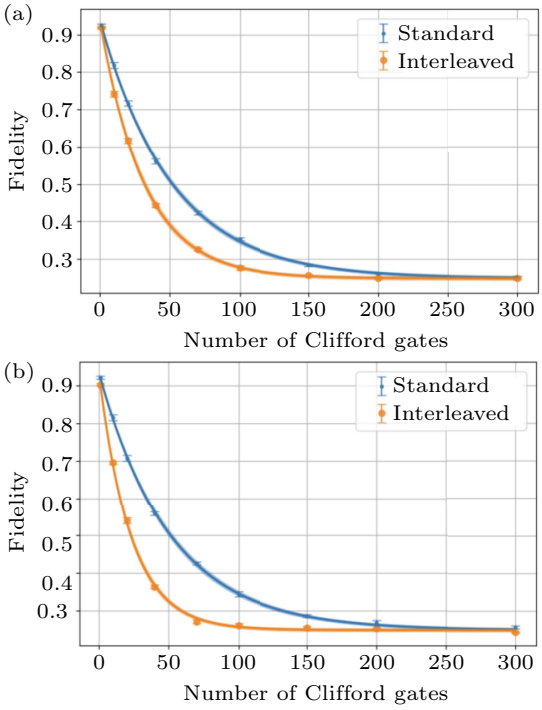



**Fig. 6.** Interleaved randomized benchmarking of the iSWAP and SWAP gates. (a) iSWAP gate. The fitted parameters are $\alpha = 0.988$ and $\alpha_\text{c} = 0.995$, where $\alpha$ is the depolarizing parameter and $\alpha_\text{c}$ is the ratio of the depolarizing parameter of interleaved RB to that of standard RB. (b) SWAP gate. The fitted parameters are $\alpha = 0.979$ and $\alpha_\text{c} = 0.983$. The horizontal axis represents the length of the Clifford gate sequence, while the vertical axis denotes the fidelity of the gate under test. The legend labels 'standard' and 'interleaved' correspond to standard randomized benchmarking and interleaved randomized benchmarking, respectively.

**Table 2.** Results of implementing the iSWAP gate and SWAP gates.

| | Gate Time (ns) | | Fidelity | |
|---|---|---|---|---|
| | iSWAP | SWAP | iSWAP | SWAP |
| Transmon | 647 | 935 | 99.2% | 97.9% |
| Fluxonium | 439 | 656 | 99.5% | 98.3% |

## 4. Error budget of the $\text{CCR}_{\pi/4}$ gate

In this section, we analyze the error budget of the $\text{CCR}_{\pi/4}$ gate. Errors can be categorized into coherent and incoherent types.[32] The coherent error is defined by $r_\text{coh} = 1 - F$, where $F$ is derived according to Eq. (27). It can be further decomposed into the leakage error $r_\text{leak}$ and the imperfect unitary error $r_\text{unitary}$.

The leakage error denotes the undesired population transfer of a qubit state from the computational subspace to non-computational levels during evolution, and it can be expressed as

$$r_\text{leak} = 1 - \frac{1}{4}\text{Tr}(U_\text{CCR}^\dagger U_\text{CCR}). \quad (34)$$

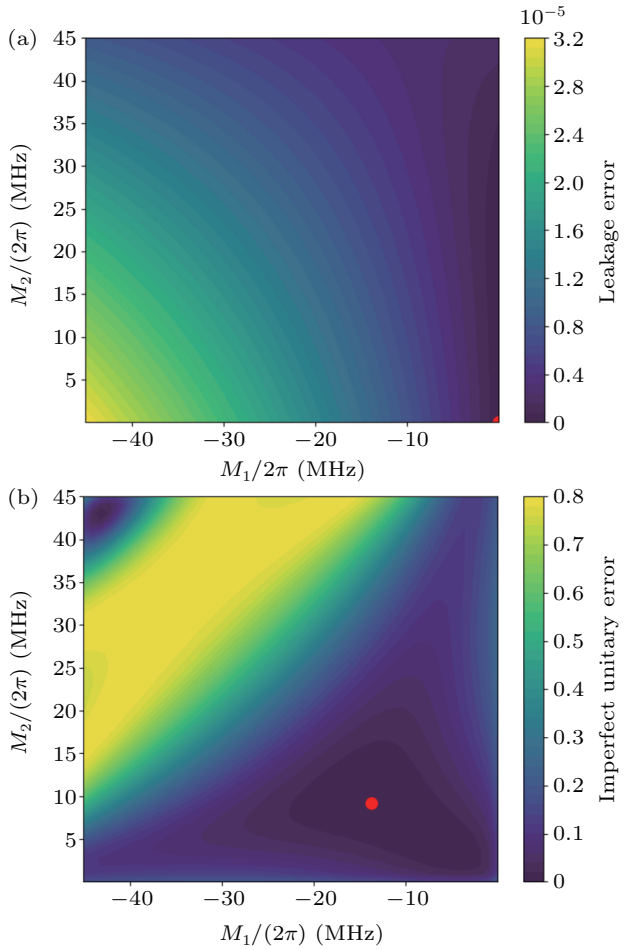



**Fig. 7.** Decomposition of the coherent error. (a) The leakage error, (b) the imperfect unitary error for various $(M_1, M_2)$ configurations. For the leakage error, the minimal value $10^{-9}$ is achieved at $(-0.001\ \text{MHz}, 0.001\ \text{MHz})$. For the imperfect unitary error, the minimal value $1.033 \times 10^{-4}$ is achieved at $(-13.78\ \text{MHz}, 9.18\ \text{MHz})$. Red dots in the figure denote the locations of the minimal values.

The imperfect unitary error, which arises when the implemented gate deviates from the target gate, can be calculated as

$$r_{\text{unitary}} = 1 - \frac{1}{16}\left|\text{Tr}(U_{\text{target}}^{\dagger} U_{\text{CCR}})\right|^2. \tag{35}$$

Figure 7 illustrates how the leakage error and the imperfect unitary error vary with $M_1$ and $M_2$. We find that the leakage error remains at or below the order of $10^{-5}$, indicating that it constitutes a negligible fraction of the total coherent error, while the imperfect unitary error dominates. The coherent error can be suppressed by adjusting the gate duration and drive frequencies. In this work, we investigate the dependency of the fidelity on the gate duration and identify the optimal frequency configuration at the corresponding optimal gate duration.

Besides the coherent error, the incoherent error induced by relaxation and dephasing can further degrade the gate performance. For the $\sqrt{\text{iSWAP}}$ gate, the incoherent error can be expressed as

$$r_{\text{incoh}}^{\sqrt{\text{iSWAP}}} \approx \frac{1}{5}\sum_{l=1}^{2}\left(\frac{1}{T_{1,l}} + \frac{2}{T_{2,l}}\right) t_{\text{g}}, \tag{36}$$

where $T_{1,l}$ and $T_{2,l}$ denote the relaxation and dephasing times of the $l$th qubit, respectively. The derivation of this formula follows the procedure for the iSWAP gate in Ref. [37], with the key difference being that the gate time here is half that of the iSWAP gate. Since the $\text{CCR}_{\pi/4}$ gate is locally equivalent to the $\sqrt{\text{iSWAP}}$ up to single-qubit rotations, and the average gate fidelity is invariant under local unitaries, its incoherent error can be evaluated using a similar expression

$$r_{\text{incoh}}^{\text{CCR}} \approx \frac{1}{5}\sum_{l=1}^{2}\left(\frac{1}{T_{1,l}} + \frac{2}{T_{2,l}}\right) t_{\text{g}}, \tag{37}$$

where the values of $T_{1,l}$ and $T_{2,l}$ are listed in Table 2. As a result, the incoherent error of the $\text{CCR}_{\pi/4}$ gate is $r_{\text{incoh}}^{\text{CCR}} \approx 0.1\%$. In this work, we mitigate the effect of decoherence by employing a gate duration of 112 ns rather than a longer operation time.

## 5. Conclusion

In summary, we demonstrate a high-performance CCR gate based on fluxonium qubits, exhibiting significant improvements over conventional transmon-based approaches. In our scheme, the $ZX$ and $XZ$ interactions are stronger than those in transmon implementations, facilitating faster gate operations under comparable conditions. We further investigate the effects of drive amplitudes and qubit frequency detuning on the CCR gate's fidelity across various gate durations, finding that the maximum fidelity is achieved at a duration of 112 ns. With optimal parameters, we realize an iSWAP gate with a duration of 439 ns and a fidelity of 99.5%, as well as a SWAP gate with a duration of 656 ns and a fidelity of 98.3%. Additionally, we analyze the error budget of the $\text{CCR}_{\pi/4}$ gate and find that the imperfect unitary error is the dominant contribution. Our results highlight the potential of the fluxonium qubit as a scalable platform for high-fidelity two-qubit gates.

## Appendix A: Derivation of the effective Hamiltonian of the fluxonium CCR gate

The system Hamiltonian is

$$\begin{aligned}\hat{H} = &-\frac{\hbar\omega_A}{2}\hat{\sigma}_z^A - \frac{\hbar\omega_B}{2}\hat{\sigma}_z^B + J_C\hat{n}_A\hat{n}_B \\ &+E_1\cos(\omega_{d1}t)\hat{n}_A + E_2\cos(\omega_{d2}t)\hat{n}_B,\end{aligned} \tag{A1}$$

where

$$\hat{n}_A = \begin{pmatrix} 0 & p \\ -p & 0 \end{pmatrix}, \quad \hat{n}_B = \begin{pmatrix} 0 & q \\ -q & 0 \end{pmatrix}. \tag{A2}$$

We divide $\hat{H}$ into two parts: the free plus coupling Hamiltonian

$$\hat{H}_0 = -\frac{\hbar\omega_A}{2}\hat{\sigma}_z^A - \frac{\hbar\omega_B}{2}\hat{\sigma}_z^B + J_C\hat{n}_A\hat{n}_B, \tag{A3}$$

and the drive Hamiltonian

$$\hat{H}_1 = E_1\cos(\omega_{d1}t)\hat{n}_A + E_2\cos(\omega_{d2}t)\hat{n}_B. \tag{A4}$$

Assuming the qubit eigenstates are $|0\rangle_A$, $|1\rangle_A$, $|0\rangle_B$, $|1\rangle_B$, the eigenstates of $\hat{H}_0$ are $|00\rangle$, $|01\rangle$, $|10\rangle$, and $|11\rangle$, which are generally entangled due to the coupling $J_C$. In this entangled basis, $\hat{H}_0$ has eigenenergies $\pm\xi$ and $\pm\epsilon$, where

$$\begin{aligned}\xi &= \frac{1}{2}\sqrt{\hbar^2(\omega_A+\omega_B)^2+4(J_C pq)^2},\\ \epsilon &= \frac{1}{2}\sqrt{\hbar^2(\omega_A-\omega_B)^2+4(J_C pq)^2}.\end{aligned} \tag{A5}$$

The eigenstate of the system can be written as

$$\begin{aligned}|\Psi(t)\rangle &= c_{uu}(t)\exp\left(\frac{\mathrm{i}\xi t}{\hbar}\right)|uu\rangle + c_{ud}(t)\exp\left(\frac{-\mathrm{i}\epsilon t}{\hbar}\right)|ud\rangle\\ &+c_{du}(t)\exp\left(\frac{\mathrm{i}\epsilon t}{\hbar}\right)|du\rangle + c_{dd}(t)\exp\left(\frac{-\mathrm{i}\xi t}{\hbar}\right)|dd\rangle.\end{aligned} \tag{A6}$$

Applying the Schrödinger equation gives differential equations for the coefficients $c_{ij}(t)$ (see Eq. (A6) in the main text). The matrix elements $\langle ab|\hat{n}_{A(B)}|cd\rangle$ are calculated following Ref. [32]. After solving these equations and performing perturbative expansions, we obtain the Hamiltonian

$$\begin{aligned}\hat{H} &= (\hbar\omega_{\mathrm{p}}-\xi-\epsilon)\frac{IZ}{2}+(\hbar\omega_{\mathrm{p}}-\xi+\epsilon)\frac{ZI}{2}\\ &+\frac{E_1}{2}(n^A_{00,01}+n^A_{10,11})\left[\cos(\omega_m t)\frac{IX}{2}-\sin(\omega_m t)\frac{IY}{2}\right]\\ &+\frac{E_2}{2}(n^B_{00,01}+n^B_{10,11})\left[\cos(\omega_m t)\frac{IX}{2}+\sin(\omega_m t)\frac{IY}{2}\right]\\ &+\frac{E_1}{2}(n^A_{00,10}+n^A_{01,11})\left[\cos(\omega_m t)\frac{XI}{2}-\sin(\omega_m t)\frac{YI}{2}\right]\\ &+\frac{E_2}{2}(n^B_{00,10}+n^B_{01,11})\left[\cos(\omega_m t)\frac{XI}{2}+\sin(\omega_m t)\frac{YI}{2}\right]\\ &+\frac{E_1}{2}(n^A_{00,10}-n^A_{01,11})\frac{XZ}{2}+\frac{E_2}{2}(n^B_{00,01}-n^B_{10,11})\frac{ZX}{2}\\ &+\frac{E_1}{2}(n^A_{00,01}-n^A_{10,11})\frac{ZX}{2}+\frac{E_2}{2}(n^B_{00,10}-n^B_{01,11})\frac{XZ}{2}\\ &+\left[\frac{E_1 r_1}{2}(n^A_{00,10}-n^A_{01,11})+\frac{E_2 r_2}{2}(n^B_{00,01}-n^B_{10,11})\right]\frac{ZZ}{2}\\ &+\left[\frac{E_1 r_2}{2}(n^A_{00,01}-n^A_{10,11})+\frac{E_2 r_1}{2}(n^B_{00,10}-n^B_{01,11})\right]\\ &\times\cos(2\omega_m t)\frac{ZZ}{2}.\end{aligned} \tag{A7}$$

High-frequency terms are discarded to finally obtain the effective Hamiltonian (7).

## References


[1] You J Q and Nori F 2005 *Phys. Today* **58** 42
[2] Clarke J and Wilhelm F K 2008 *Nature* **453** 1031
[3] Krantz P, Kjaergaard M, Yan F, Orlando T P, Gustavsson S and Oliver W D 2019 *Appl. Phys. Rev.* **6**
[4] Blais A, Grimsmo A L, Girvin S and Wallraff A 2021 *Rev. Mod. Phys.* **93** 025005
[5] Shnirman A, Schön G and Hermon Z 1997 *Phys. Rev. Lett.* **79** 2371
[6] Nakamura Y, Pashkin Y A and Tsai J S 1999 *Nature* **398** 786
[7] Mooij J E, Orlando T P, Levitov L, Tian L, van der Wal C H and Lloyd S 1999 *Science* **285** 1036
[8] Dmitriev A Y and Astafiev O V 2021 *Appl. Phys. Lett.* **119**
[9] Martinis J M, Nam S, Aumentado J and Urbina C 2002 *Phys. Rev. Lett.* **89** 117901
[10] Martinis J M 2009 *Quantum Inf. Process.* **8** 81
[11] Xiang Z L, Ashhab S, You J Q and Nori F 2013 *Rev. Mod. Phys.* **85** 623
[12] Koch J, Yu T M, Gambetta J, Houck A A, Schuster D I, Majer J, Blais A, Devoret M H, Girvin S M and Schoelkopf R J 2007 *Phys. Rev. A* **76** 042319
[13] Roth T E, Ma R and Chew W C 2023 *IEEE Antennas Propag. Mag.* **65** 8
[14] Manucharyan V E, Koch J, Glazman L I and Devoret M H 2009 *Science* **326** 113
[15] Bao F, Deng H, Ding D, Gao R, Gao X, Huang C, Jiang X, Ku H S, Li Z, Ma X, Ni X, Qin J, Song Z, Sun H, Tang C, Wang T, Wu F, Xia T, Yu W, Zhang F, Zhang G, Zhang X, Zhou J, Zhu X, Shi Y, Chen J, Zhao H H and Deng C 2022 *Phys. Rev. Lett.* **129** 010502
[16] Lin Y H, Nguyen L B, Grabon N, San Miguel J, Pankratova N and Manucharyan V E 2018 *Phys. Rev. Lett.* **120** 150503
[17] Nguyen L B, Lin Y H, Somoroff A, Mencia R, Grabon N and Manucharyan V E 2019 *Phys. Rev. X* **9** 041041
[18] Zhang H, Chakram S, Roy T, Earnest N, Lu Y, Huang Z, Weiss D, Koch J and Schuster D I 2021 *Phys. Rev. X* **11** 011010
[19] Rower D A, Ding L, Zhang H, Hays M, An J, Harrington P M, Rosen I T, Gertler J M, Hazard T M, Niedzielski B M, Schwartz M E, Gustavsson S, Serniak K, Grover J A and Oliver W D 2024 *PRX Quantum* **5** 040342
[20] Bothara G, Das S, Salunkhe K V, Chand M, Deshmukh J, Patankar M P and Vijay R 2025 *APL Quantum* **2** 026103
[21] Nielsen M A and Chuang I L 2010 Quantum Computation and Quantum Information (Cambridge : Cambridge University Press)
[22] Paraoanu G S 2006 *Phys. Rev. B* **74** 140504
[23] Rigetti C and Devoret M 2010 *Phys. Rev. B* **81** 134507
[24] Córcoles A D, Gambetta J M, Chow J M, Smolin J A, Ware M, Strand J, Plourde B L T and Steffen M 2013 *Phys. Rev. A* **87** 030301
[25] Itoko T, Malekakhlagh M, Kanazawa N and Takita M 2024 *Phys. Rev. Appl.* **21** 034018
[26] Kandala A, Mezzacapo A, Temme K, Takita M, Brink M, Chow J M and Gambetta J M 2017 *Nature* **549** 242
[27] Takita M, Cross A W, Córcoles A, Chow J M and Gambetta J M 2017 *Phys. Rev. Lett.* **119** 180501
[28] Sheldon S, Magesan E, Chow J M and Gambetta J M 2016 *Phys. Rev. A* **93** 060302
[29] Magesan E and Gambetta J M 2020 *Phys. Rev. A* **101** 052308
[30] Malekakhlagh M, Magesan E and McKay D C 2020 *Phys. Rev. A* **102** 042605
[31] Chow J M, Córcoles A D, Gambetta J M, Rigetti C, Johnson B R, Smolin J A, Rozen J R, Keefe G A, Rothwell M B, Ketchen M B and Steffen M 2011 *Phys. Rev. Lett.* **107** 080502
[32] Nesterov K N, Wang C, Manucharyan V E and Vavilov M G 2022 *Phys. Rev. Appl.* **18** 034063
[33] Dogan E, Rosenstock D, Le Guevel L, Xiong H, Mencia R A, Somoroff A, Nesterov K N, Vavilov M G, Manucharyan V E and Wang C 2023 *Phys. Rev. Appl.* **20** 024011
[34] Heya K and Kanazawa N 2021 *PRX Quantum* **2** 040336
[35] Nguyen L B, Koolstra G, Kim Y, Morvan A, Chistolini T, Singh S, Nesterov K N, Jünger C, Chen L, Pedramrazi Z, Mitchell B K, Kreikebaum J M, Puri S, Santiago D I and Siddiqi I 2022 *PRX Quantum* **3** 037001
[36] Javadi-Abhari A, Treinish M, Krsulich K, Wood C J, Lishman J, Gacon J, Martiel S, Nation P D, Bishop L S, Cross A W, Johnson B R and Gambetta J M 2024 *Quantum Computing with Qiskit* (Cambridge: Cambridge University Press)
[37] Sete E A, Tripathi V, Valery J A, Lidar D and Mutus J Y 2024 *Phys. Rev. Appl.* **22** 014059